Influence of Aerodynamics and Proximity Effects in Quadrotor Flight

Caitlin Powers, Daniel Mellinger, Aleksandr Kushleyev, Bruce Kothmann, Vijay Kumar

Abstract The dynamic response and performance of a micro UAV is greatly influenced by its aerodynamics which in turn is affected by the interactions with features in the environment in close proximity. In the paper we address the modeling of quadrotor robots in different flight conditions that include relative wind velocity and proximity to the ground, the ceiling and other robots. We discuss the incorporation of these models into controllers and the use of a swarm of robots to map features in the environment from variations in the aerodynamics.

1 Introduction

With recent advances in aerial robotics it is now possible to design and build vehicles that can fly autonomously in three-dimensional, cluttered, indoor environments. However, flying close to such obstacles as pillars, through windows, close to the

Caitlin Powers
GRASP Laboratory, University of Pennsylvania, Philadelphia, PA 19104 USA e-mail: cpow@seas.upenn.edu

Daniel Mellinger
GRASP Laboratory, University of Pennsylvania, Philadelphia, PA 19104 USA e-mail: dmel@seas.upenn.edu

Aleksandr Kushleyev
GRASP Laboratory, University of Pennsylvania, Philadelphia, PA 19104 USA e-mail: akushley@seas.upenn.edu

Bruce Kothmann
GRASP Laboratory, University of Pennsylvania, Philadelphia, PA 19104 USA e-mail: kothmann@seas.upenn.edu

Vijay Kumar
GRASP Laboratory, University of Pennsylvania, Philadelphia, PA 19104 USA e-mail: kumar@seas.upenn.edu

ground or near ceilings changes the dynamics of the vehicle because of changes in the aerodynamics. For autonomous flight, it is essential to understand and anticipate these changes and develop controllers that are responsive and adapt to these changes. Indeed, we want to be to exploit the asymmetry introduced by features in the environment the same way birds are able to do during flight [8].

Nature also offers many benefits of flying in flocks in close proximity. Experimental evidence suggests benefits of higher efficiency [7], superior localization [6], better decision making [5], and survival [15]. Similar benefits can be potentially realized in groups of aerial robots. Once again it essential to be able to model the effects of flight in close proximity and develop controllers that are informed by these models.

We are interested in autonomous micro helicopters, exemplified by coaxial rotor crafts [3], ducted fans [16], quadrotors [4] and hexarotors, and specifically in small quadrotors such as the ones recently demonstrated in [11] that weigh less than 100 grams, are less than 0.25 meters, and are agile in three-dimensional flight. In quadrotors, the lift generated by the aircraft depends on the flow conditions near the propellers and the propeller speeds. These are coupled with the rigid body dynamics, the dynamics of the propeller and the motor dynamics. In a quadrotor, an onboard motor controller is used to control the motor current with feedback loops that incorporate information from onboard gyros and accelerometers and position relative to either features in the environment or with respect to a global coordinate system. However, the actual motor speed and the effective forces and moments acting on the airframe are a complex function of the aerodynamics. It is this function that must be properly understood and modeled in order to produce agile flight.

Previous investigation of quadrotor aerodynamics has shown the importance of considering aerodynamics in quadrotor control [9]. We take a different approach here to incorporate blade element theory. We choose this approach to eliminate power considerations as our system is fundamentally controlled at the level of rotor speed.

In this paper, we describe the modeling of a single rotor and the robot (Sec. 2) and the measured thrust versus speed in different flow conditions with our experimental test rig and in-flight data (Sec. 5). We show that the lift produced by a propeller is affected by relative wind velocity and by proximity to the ground and ceiling and develop empirical models that lend themselves to control.

2 Dynamics and Control

The dynamic model and control for the micro quadrotor is based on the approach in [13]. As shown in Figure 1, we consider a body-fixed frame $\mathscr{B}$ aligned with the principal axes of the quadrotor (unit vectors $\mathbf{b}_i$) and an inertial frame $\mathscr{A}$ with unit vectors $\mathbf{a}_i$. $\mathscr{B}$ is described in $\mathscr{A}$ by a position vector $\mathbf{r}$ to the center of mass C and a rotation matrix R. In order to avoid singularities associated with parameterization, we use the full rotation matrix to describe orientations. The angular velocity of

the quadrotor in the body frame, given by $\hat{\omega}_B = R^T \dot{R}$, where $\hat{}$ denotes the skew-symmetric matrix form of the vector.

As shown in Fig. 1, the four rotors are numbered 1-4, with odd numbered rotors having a pitch that is opposite to the even numbered rotors. The angular speed of the rotor is ω_i. The resulting thrust, T_i, and the reaction moment, M_i, are given by:

$$T_i = k_T \omega_i^2,\ M_i = k_M \omega_i^2 \tag{1}$$

where the constants k_T and k_M are empirically determined for a propeller in still air. For our micro quadrotor, the motor dynamics have a time constant less than 10 msec and are much faster than the time scale of rigid body dynamics and aerodynamics. Thus we neglect the dynamics and assume T_i and M_i can be instantaneously changed. Therefore the control input to the system, $\mathbf{u}$, consists of the net thrust in the $\mathbf{b}_3$ direction, $u_1 = \Sigma_{i=1}^4 T_i$, and the moments in $\mathscr{B}$, $[u_2, u_3, u_4]^T$, given by:

$$\mathbf{u} = \begin{bmatrix} k_T & k_T & k_T & k_T \\ 0 & k_T L & 0 & -k_T L \\ -k_T L & 0 & k_T L & 0 \\ k_M & -k_M & k_M & -k_M \end{bmatrix} \begin{bmatrix} \omega_1^2 \\ \omega_2^2 \\ \omega_3^2 \\ \omega_4^2 \end{bmatrix} \tag{2}$$

where L is the distance from the axis of rotation of the propellers to the center of the quadrotor.

The Newton-Euler equations of motion are given by:

$$m\ddot{\mathbf{r}} = -mg\mathbf{a}_3 + u_1 \mathbf{b}_3 \tag{3}$$

$$\dot{\omega} = \mathscr{I}^{-1} \left[-\omega \times \mathscr{I}\omega + \begin{bmatrix} u_2 \\ u_3 \\ u_4 \end{bmatrix} \right] \tag{4}$$

where $\mathscr{I}$ is the moment of inertia matrix along $\mathbf{b}_i$. The main error in this model comes from the simplistic assumption underlying (1) that the lift force and drag moments are directly proportional to the square of the motor speed. In reality they are complex functions of the motor speed and environmental conditions.

Given a desired trajectory, $\mathbf{r}_T$, the controller derives the input u_1 based on position and velocity errors:

$$u_1 = (-K_p \mathbf{e}_p - K_v \mathbf{e}_v + mg\mathbf{a}_3) \cdot \mathbf{b}_3 \tag{5}$$

where $\mathbf{e}_p = \mathbf{r} - \mathbf{r}_T$ and $\mathbf{e}_v = \dot{\mathbf{r}} - \dot{\mathbf{r}}_T$. From the desired acceleration and a chosen yaw angle the total desired orientation can be found. As described in [13], the desired moments are expressed as a function of an orientation error, $\mathbf{e}_R$, and an angular velocity error, $\mathbf{e}_\omega$:

$$[u_2, u_3, u_4]^T = -K_R \mathbf{e}_R - K_\omega \mathbf{e}_\omega, \tag{6}$$

where K_R and K_ω are diagonal gain matrices. Finally we compute the desired rotor speeds to achieve the desired $\mathbf{u}$.

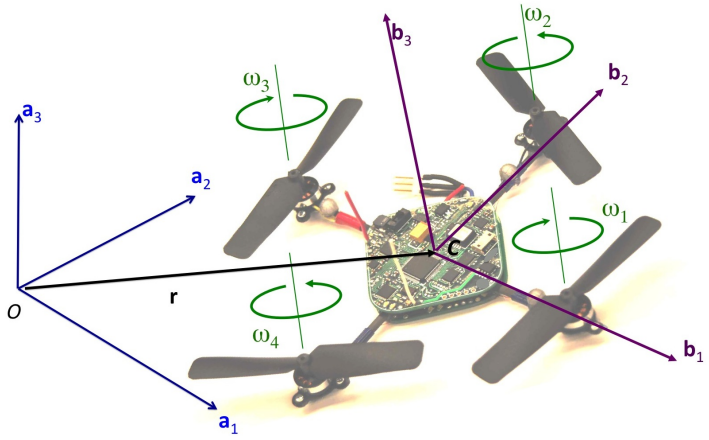

Fig. 1: The reference frames and propeller numbering convention.

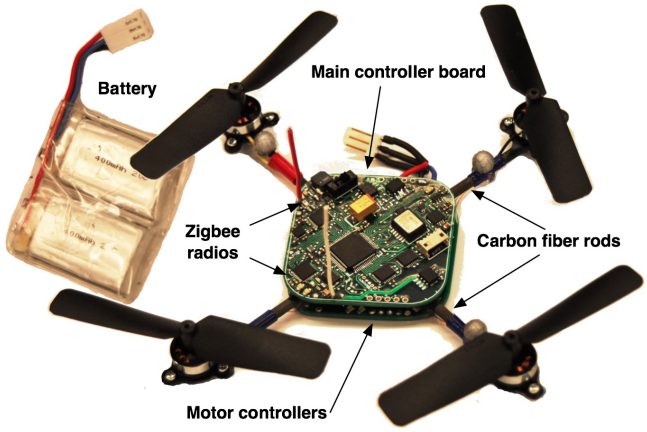

Fig. 2: The kQuadNano [1]

3 Experiment Testbed

For the experiments presented in this work we use the kQuadNano developed by KMel Robotics [1] shown in Figure 2. The vehicle uses four 8 cm diameter fixed-pitch propellers. The vehicle propeller-tip-to-propeller-tip distance is 21 cm and the total weight with a battery is about 76 grams.

We use a Vicon motion capture system [2] to sense the position of each vehicle at 100 Hz. This data is streamed over a gigabit ethernet network to a desktop base station. High-level control is done in MATLAB on the base station which sends

commands to each quadrotor at 100 Hz. The base station sends, via custom radio modules, the desired commands, containing orientation, thrust, angular rates and attitude controller gains to the individual quadrotors. The onboard rate gyros and accelerometer are used to estimate the orientation and angular velocity of the craft. The main microprocessor runs an attitude controller and sends the desired propeller speeds to each of the four motor controllers at 600 Hz. A more detailed description of the experimental setup is presented in [12].

Experiments were also performed using a custom thrust test rig. The test rig includes a load cell from Transducer Technologies rated for 100 g for measuring thrust and electronic instrumentation for data collection. The rotor for testing is mounted on a rod and attached to a lever which transmits the thrust to the load cell. The test rig is pictured in Fig. 3a.

4 Effect of Proximity to Horizontal Surfaces

It is known that rotorcraft operating near surfaces experience a "ground effect" where the rotors produce more thrust per unit power compared to flight at a large distance from the ground. One proposed mathematical description of ground effect [10], based on the method of images, is

$$\frac{T}{T_\infty} = \frac{1}{1-(\frac{R}{4z})^2} \tag{7}$$

Here R is the radius of the rotor, z is the vertical distance from the ground, T is the thrust produced by the propeller in ground effect, and T_∞ is the thrust produced at the same power outside of ground effect. Note that for $\frac{z}{R} = 2$ the predicted ratio

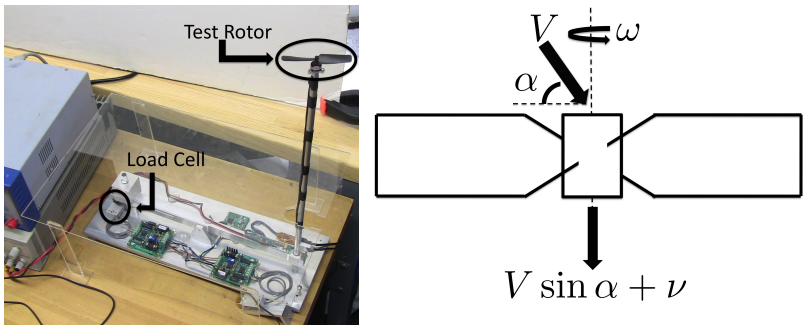

(a) Thrust Test Rig (b) Diagram of Rotor

Fig. 3: The test rig (left) and a schematic showing the relative wind speed and the angle of attack, α.

between T and T_∞ is just 1.016. Therefore, this formula predicts that ground effect is negligible when the rotor is more than one diameter off the ground, $\frac{z}{R} > 2$ [10].

In order to test the ground effect in flight, the quadrotor was commanded to hover at a range of distances above the ground for 10 seconds and the average rotor speed required to maintain hover was recorded. This test provides a relationship between height and angular speed required to produce a constant thrust. The data for this test is shown in Fig. 4a. The general trend predicted by (7) is observed in this data since the propeller requires a lower rotor speed to maintain hover at lower heights. However, in this data the ground effect can be observed up to about 20 cm ($\frac{z}{R} = 5$) which is significantly higher than (7) predicts.

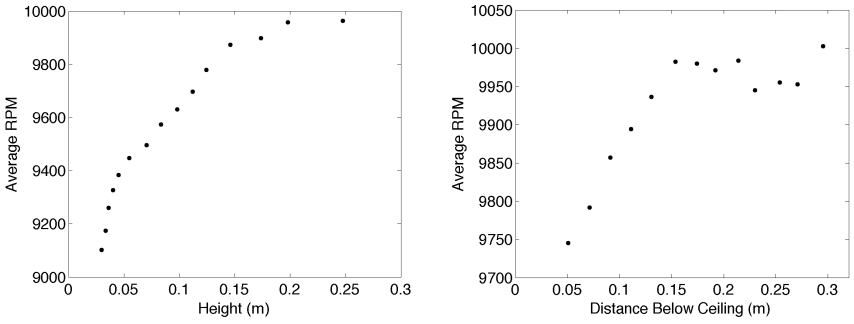

(a) Ground Effect (b) Ceiling Effect

Fig. 4: Effect of proximity to horizontal surfaces. Each data point is based on 10 seconds of hover data for a vehicle with propellers with $R = 4$ cm. Note that noise could likely be reduced by averaging data for a longer time period.

Unlike larger helicopters, micro quadrotors can be used for indoor missions. This motivates the investigation of a "ceiling effect" which is present when the vehicle is close to an overhead plane. Performing a similar experiment, we found data for the ceiling effect as shown in Fig. 4b. The ceiling effect is not as large as the ground effect as observed by the smaller change in average rotor speed for the same separation. Note that while the ground effect pushes the vehicle away from the ground, the ceiling effect pulls the vehicle towards the ceiling which can cause a crash in the worst case.

5 Aerodynamics of Vertical and Forward Flight

The thrust produced by a rotor in flight is in general a function of the relative velocity between the rotor and the surrounding air, V, as well as the angle of attack α as shown in Fig. 3b. For the situation where $\alpha = \frac{\pi}{2}$, the craft is said to be in climb.

The velocity of the slipstream increases as it passes through the rotor. We refer to this additional velocity imparted by the rotor as the induced velocity, v. Momentum theory analysis relates the additional kinetic energy of the air at an infinite distance from the rotor to the thrust, and provides us with an expression for the thrust in climb or descent [10]:

$$T = \dot{m}w = 2\rho A v \left| V + v \right| \tag{8}$$

Here T is the rotor thrust, ρ is the density of air, A is the area swept by the rotor, $\dot{m}$ is the mass flow through a disc of area A and w is the velocity of the air an infinite distance after it has passed through the rotor. In order to have a complete system of equations, we turn to blade element theory to find another expression for the thrust in climb from a rotor [10]:

$$T = \frac{\rho abc\omega^2 R^3}{4}\left(\theta_{tip} - \frac{V+v}{\omega R}\right) \tag{9}$$

Here ω is the rotor speed, R is the radius of the rotor, θ_{tip} is the pitch angle at the blade tip, a is the lift curve slope, b is the number of blades on the rotor, and c is the blade chord. a, b, c, and θ_{tip} are functions of the rotor geometry alone. Note that if V is 0, the induced velocity is equal to $\sqrt{\frac{T}{2\rho A}}$, and this expression becomes the familiar $T = k\omega^2$ in (1).

Given (8) and (9), a climb velocity V and angular speed ω we can solve a quadratic equation for v and then use either expression to find the thrust. In (9) we have two groups of terms describing the geometry of the rotor which depend on assumptions about the rotor construction, e.g., that it is ideally twisted and has a constant chord. By grouping the terms we can rewrite (9) as

$$T = k_1\omega^2 + k_2(V+v)\omega \tag{10}$$

where k_1 and k_2 are determined by the rotor geometry and the density of air. One approach for finding these constants would be to measure the physical parameters of the propeller, however, this approach suffers from reliance on many assumptions about the blade geometry. Instead we choose to empirically determine these constants. We collect test rig andin-flight data to find the constants which best describe the experimental data. The in-flight test was performed by commanding a micro quadrotor to ascend or descend at a constant velocity. We then measured the steady state rotor speed to determine ω required to produce a thrust of mg at the given vertical velocity. Several data points were collected for each velocity by adding small amounts of weight to the quadrotor to vary the required thrust. In addition, measurements from the thrust test rig provide data for a variety of rotor speed and thrust combinations. We use the thrust from all these trials to compute the induced velocity from (8). Next we note that the unknowns appear linearly in (10). We combine the data from all trials and use a linear least squares method to determine the constants which best fit the data. The experimental data and the fitted model is shown in Fig. 5. The maximum error between the fit and the experimental data is .64 g over all trials.

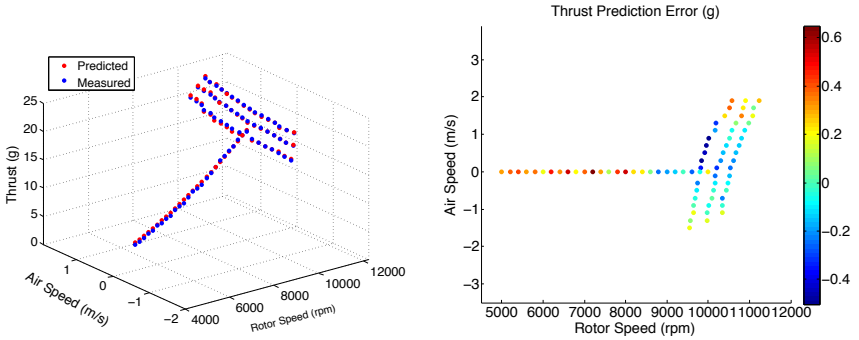

Fig. 5: Experimental Data and Fitted Model for Thrust as a Function of Air and Rotor Speed

Once we have constants k_1 and k_2, we can predict the thrust at a given V and ω using our model following a two step process:

1. First, solve for v by finding the roots of the quadratic equation formed from (8) and (9). Choose the positive root as the reasonable physical induced velocity.
2. Substitute v into equation (9) to find the predicted thrust.

We can implement this procedure in reverse to find the ω which produces a given thrust at the current vertical velocity. The inclusion of this approach in the control law improves tracking performance as shown in Sec. 7.

In forward flight, we must add angle of attack α to our model as shown in Fig. 3b. The equations for thrust become

$$T = 2\rho A v \sqrt{V^2 + 2Vv\sin\alpha + v^2} \tag{11}$$

and

$$T = \frac{\rho abc\omega^2 R^3}{2}\left(\frac{\theta}{3} + \frac{V^2\cos^2\alpha\theta}{2\omega^2R^2} + \frac{V\sin\alpha + v}{2\omega R}\right) \tag{12}$$

where θ is the pitch angle and is a function of rotor geometry alone as we are considering fixed pitch rotors [10]. The equation for v is now a fourth order polynomial instead of a quadratic. We characterized the dependence of thrust on rotor speed using the thrust test rig for five angles of attack and four wind speeds at each angle. The total thrust produced by the rotor decreases notably with increased wind speed in a given direction. As the angle of attack increases, the thrust variation due to wind speed decreases, as the component of wind velocity perpendicular to the rotor increases more slowly. At $\alpha = 30°$, the effect of wind speed has decreased significantly, such that the largest observed difference between the no wind condition and the highest wind speed condition is 1 g.

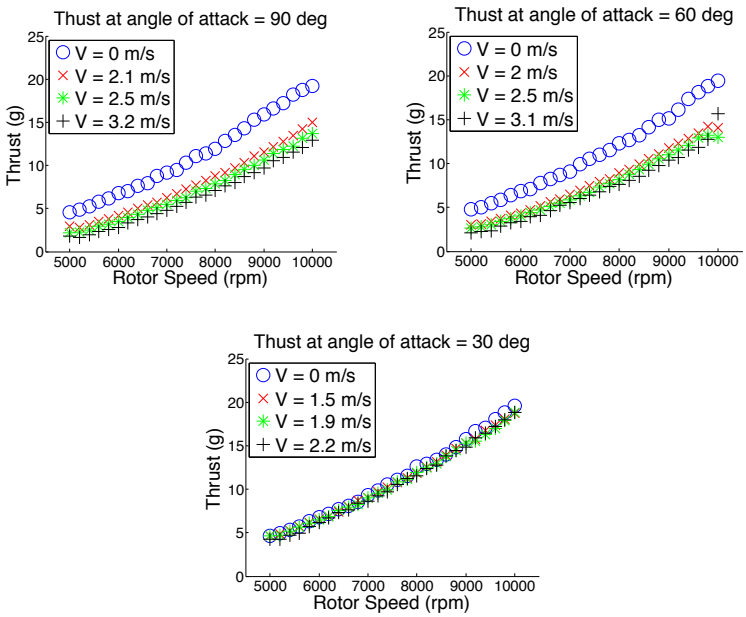

Fig. 6: The dependence of thrust on rotor speed and wind speed.

While the data from the test rig is consistent with our model, it is not completely consistent with the data collected in free flight. We suspect this is primarily due to our inability to reproduce the flow conditions during free flight. The data from the test rig in the no wind condition is consistent with the in flight data and so was used in fitting the model. This is a subject of ongoing investigation as we continue to determine the best model for wind effects on small aerial vehicles.

6 Effect of Neighboring Vehicles

Micro quadrotors can be used in teams to cooperate to accomplish tasks that they individually cannot perform. If we are to reliably control formations of vehicles, we should be aware of the effects that neighboring quadrotors have on one another. It is known that vehicles have difficulty flying in the downwash of other vehicles [14]. Here we investigate the effect of nearby quadrotors in the same plane. We flew quadrotors along the same 3 meter long trajectory but in several scenarios as illustrated in Fig. 7. For the first scenario (quadrotor 1) we evaluated the performance of a single quadrotor flying by itself without neighbors. For the second scenario (quadrotors 2, 3 and 4) we investigated the effect of quadrotors traveling in close proximity in the same direction. And for the final scenario (quadrotors 5, 6 and 7) we tested the effect of quadrotors traveling close together but in different directions. For each

scenario the command to an individual quadrotor was the same. Each quadrotor was commanded to start at hover, accelerate at 1 $\mathrm{m/s^2}$ to a speed of 1.5 $\mathrm{m/s}$ and then decelerate to a stop at the same acceleration all at a constant height of 1 m. Note that for the scenarios with multiple vehicles the desired separation between vehicles was set to 40 cm.

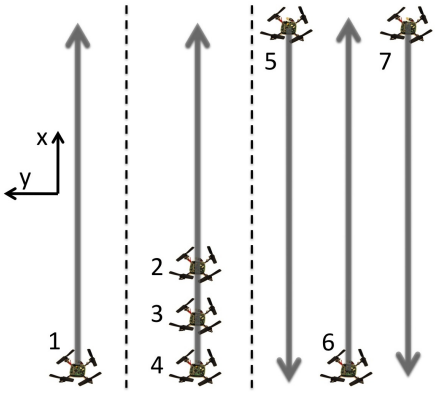

Fig. 7: Three scenarios for testing the effect of neighboring vehicles. Dotted lines separate the scenarios and arrows illustrate the commanded trajectories for the vehicles. Left: A single quadrotor. Middle: Three quadrotors moving in the same direction. Right: Three quadrotors moving in opposite directions.

Each scenario was run for 10 trials. The standard deviations in position error for each quadrotor for each trial, labeled 1-7, are shown in Fig. 8. As expected, the error is the direction of travel is the worst. There does not appear to be a significant change in any error from one configuration to another. One interesting observation is that the leading quadrotor (number 2) in the second scenario exhibits a slightly larger error in the direction of travel than the vehicles that follow it (numbers 3 and 4). We hypothesize that this is because quadrotors 3 and 4 are "drafting" quadrotor 2 and experience less aerodynamic drag which leads to slightly increased tracking performance.

7 Applications

7.1 Blind Terrain Mapping

Here we exploit the ground effect discussed in Sec. 4 to enable a team of quadrotors to build a height map of the terrain over which they fly. No sensors are required

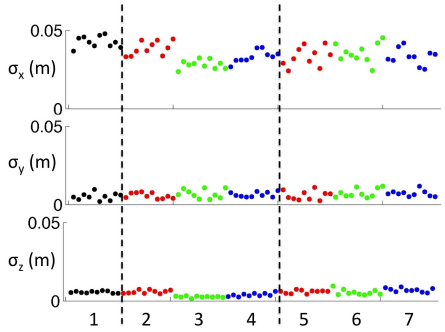

Fig. 8: Standard Deviations in Position Errors for 10 trials for each of the 3 scenarios shown in Fig. 7. The number along the x axis indicates that the 10 data points above it correspond to the trials for the vehicle number shown in Fig. 7. The dotted lines separate the three scenarios.

to build this map, only knowledge of the average rpm required to hover. At slow forward velocities, we can assume that the thrust produced is approximately thrust required to hover. We used a team of five micro quadrotors to sweep an area of varying height in the z direction at a lateral speed of 6 cm/s at a constant height of 20 cm. Vehicles flew at a separation distance of 60 cm and made four equally spaced passes through the environment. Three different 60 cm $\times$ 60 cm blocks with heights of 15 cm, 10 cm, and 6 cm were placed in the environment. We recorded the low-pass filtered rotor speed required to hover along each trajectory. This data can be used with the ground effect data shown in Fig. 4a to create a map of the terrain height underneath the vehicles. The rotor speed required to hover collected during the experiment is compared to the required rotor speed predicted from our model and the actual terrain map is shown in Fig. 9. Here darker colors represent smaller rotor speeds (taller terrain). From the data we can clearly identify the location of the tallest two blocks in the environment and somewhat identify the presence of the shortest block. Note that this approach is not likely useful for developing high-resolution ground maps with a high degree of accuracy but it is useful for getting a rough estimate of the terrain map. In addition, it may be useful in detecting sudden changes in height during mapping for verification of other sensors.

7.2 Control Compensation

Our standard quadrotor control law assumes the relationship between thrust and rotor speed is simply $T = k_T \omega^2$. However, as described in Sec. 5 this is only true when a propeller is in a stationary air field. Here we show that we can improve our controller performance by replacing the standard mapping with our model fit to the

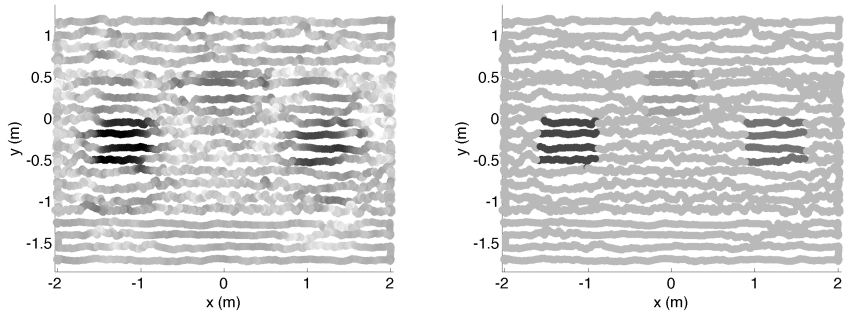

(a) Measured Rotor Speed (b) Predicted Rotor Speed

Fig. 9: Terrain Map - darker colors represent smaller rotor speeds and taller terrain

data for a quadrotor described in Sec. 5. As shown in Fig. 10a, when commanded to follow a trajectory along the z axis ascending at a velocity of 1.9 m/s, the standard uncompensated controller causes the quadrotor to lag behind the desired position up to 6 cm. This is because the propeller produces less thrust when ascending than it does when stationary for the same rotor speed. In Fig. 10b, we use a compensated controller that takes into account the vertical velocity of the vehicle in order to calculate the desired rotor speed from the desired thrust. This compensated controller reduces the maximum error to 2 cm for the same trajectory.

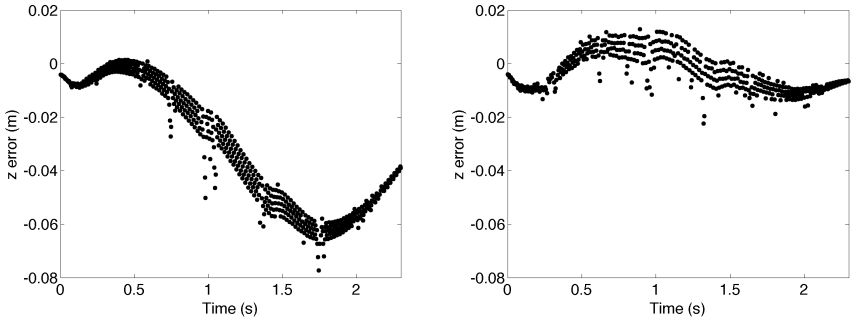

(a) Uncompensated (b) Compensated

Fig. 10: z error when following an ascending vertical trajectory at 1.9 m/s. The trajectory is 2.7 m long and the commanded acceleration when starting and stopping is 2 m/s^2.

As shown in Fig. 11, the controller compensation improved performance to a greater extent with increasing ascent velocity as expected. The compensation did not have an appreciable effect on performance in descent. This is likely because the increase in thrust during descent is not as great as the decrease in thrust during ascent for the same speed.

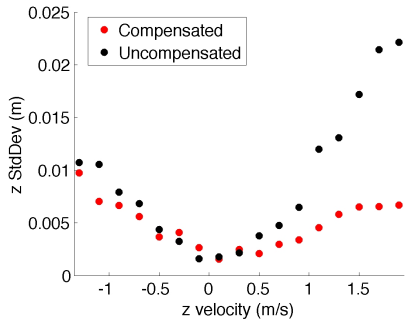

Fig. 11: Compensated and Uncompensated Controller Performance. The deviation from the trajectory decreases with added compensation.

8 Conclusions

In this paper, we address the modeling of aerodynamic effects for a small quadrotor flying through three-dimensional environments in close proximity to environmental features and neighboring quadrotors. We develop models from first principles that explain the dependence of thrust generated by the propellers on different parameters and empirically determine the coefficients for this model. We present data collected for a single rotor on a test rig as well as data collected from quadrotors in flight. We show how such models can be used to improve performance in flight and to infer the presence of ground features without additional sensors for blind mapping. A logical future step is to test the rotor performance in a larger variety of wind conditions, from strictly laminar flow to turbulent or time varying flow, in order to characterize the performance.

In the future, we hope to apply the results of this work to more complicated estimation and control problems, which will allow more robust operation of quadrotors in diverse environments. Further investigation of the influence of aerodynamics on the operation of small multi-rotor vehicles will allow engineers to make better design and control decisions. In addition, experimentally verifiable models of quadrotor aerodynamics will help enable UAVs to detect and correct for the fluctuating environments that they encounter while in operation.

References

1. KMel Robotics. http://www.kmelrobotics.com.
2. Vicon Motion Systems, Inc. http://www.vicon.com.
3. C. Bermes. *Design and dynamic modeling of autonomous coaxial micro helicopters*. Ph.D. dissertation, ETH Zurich, Zurich, Switzerland, March 2010.
4. S. Bouabdallah. *Design and Control of Quadrotors with Applications to Autonomous Flying*. PhD thesis, Ecole Polytechnique Federale de Lausanne, Lausanne, Switzerland, February 2007.
5. I. D. Couzin, J. Krause, N. R. Franks, and S. A. Levin. Effective leadership and decision-making in animal groups on the move. *Nature*, 433(7025):513–516, 2005.
6. G. Dall'Ariccia, G. Dell'Omo, D.P. Wolfer, and H-P Lipp. Flock flying improves pigeons' homing: GPS track analysis of individual flyers versus small groups. *Anim. Beh.*, 76:1165–1172, 2008.
7. F.R. Hainsworth. Precision and dynamics of positioning by canada geese flying in formation. *J. Exp. Biol.*, 128:445–462, 1987.
8. T. L. Hedrick, J. R. Usherwood, and A. A. Biewener. Wing inertia and whole-body acceleration: an analysis of instantaneous aerodynamic force production in cockatiels (nymphicus hollandi- cus) flying across a range of speeds. *J. Exp. Biol.*, 207:1689–1702, 2004.
9. H. Huang, G.M. Hoffmann, S.L. Waslander, and C.J. Tomlin. Aerodynamics and control of autonomous quadrotor helicopters in aggressive maneuvering. In *Robotics and Automation, 2009. ICRA '09. IEEE International Conference on*, pages 3277 –3282, May 2009.
10. W. Johnson. *Helicopter Theory*. Princeton University Press, Princeton, NJ, 1980.
11. V. Kumar, D. Mellinger, and A. Kushleyev. Autonomous, agile, aerial robots, 2012.
12. A. Kushleyev, D. Mellinger, and V. Kumar. Towards a swarm of agile micro quadrotors. In *Robotics: Science and Systems (RSS)*, 2012.
13. D. Mellinger and V. Kumar. Minimum snap trajectory generation and control for quadrotors. In *Proceedings of the IEEE International Conference on Robotics and Automation (ICRA)*, May 2011.
14. N. Michael, D. Mellinger, Q. Lindsey, and V. Kumar. The grasp multiple micro-uav testbed. *Robotics Automation Magazine, IEEE*, 17(3):56 –65, Sept. 2010.
15. J. Parrish and W. Hamner, editors. *Animal Groups in Three Dimensions*. Cambridge University Press, New York, 1997.
16. D. Pines and F. Bohorquez. Challenges facing future micro air vehicle development. *AIAA Journal of Aircraft*, 43(2):290–305, 2006.